End-to-End Simulation of the E163 Experiment

E. Colby for the E163 Collaboration

EPAC Comment #6: "The proposal discusses bunch lengths less than 5ps but to keep the energy spread small in the x-band linac the bunch length must be the order of 250 fs. The studies to support the generation and propagation of such a beam are not presented."

EPAC Comment #8: "The expected acceleration as proposed is small and may easily be masked by jitter or drifts. A start to end calculation of all jitter and drift sources and comparisons to the signal are essential."

EPAC Comment #9: "The 2nd phase experiment, using IFEL bunched beams, requires also a calculation of the survival of the bunching through the beam transport system."

Introduction

An end-to-end simulation of the E163 experiment has been constructed to demonstrate the production of very short, low energy spread beams of low charge, and to establish both optimal and likely performance of the first two phases of E163 under realistic conditions.

The experiments proposed in E163 have differing requirements. Phase I ("Laser Acceleration") involves precision spectrometry to demonstrate energy broadening induced by the laser interaction. Phase II ("Prebunch and Accelerate") involves optically prebunching the electron beam in an IFEL, and subsequently accelerating it using the same interaction geometry as Phase I. Phase III ("Multicell Structures") is experimentally similar to Phase II, but with larger energy gains and consequently an easier experimental measurement, and has not been simulated here.

TABLE 1: Summary of electron and laser beam parameter requirements.

Parameter	Value	Comment
Electron Beam Properties		
Bunch Charge	50 pC	
Beam Energy	60 MeV	
Transverse Emittance	< 2.5 π mm-mr	Normalized
Bunch Length	< 5 ps	FWHM
Energy Spread	< 20 keV	FWHM
Pulse Repetition Rate	10 Hz	
Laser Beam Properties (for experiment)		
Pulse Energy	1 mJ	
Pulse Wavelength	800 nm	
Pulse Length	0.1-10 ps	FWHM, variable
Pulse Repetition Rate	10 Hz	
Timing jitter w.r.t. electron beam	< 1 ps	

The experiment requirements are reproduced in Table 1, taken from the E163 proposal. The tightest of the experimental requirements are on the energy spread and timing jitter. RF-induced energy spread in the x-band accelerating sections of the NLCTA will require short electron bunches, on the order of 0.1 mm RMS, as will be discussed below. Obtaining such short bunches from an RF gun is straightforward at reduced charge, particularly when transverse emittance requirements are not demanding, as is the case for E163.

The expected amplitude of the laser-induced energy modulation is the dominant factor determining limits on the energy spread and timing jitter. Table 2 (taken from the EPAC presentation) summarizes the expected strength of the laser interaction. The parameters listed under the "Values Now" column have been used in the calculations that follow.

TABLE 2. Summary of laser interaction parameters and expected peak interaction strength. Values in the "Values Now" column are used in calculations in this paper.

Parameter	Symbol	Value in Future	Values Now	Comment
Electron Energy	E_e	60 MeV	60 MeV	
Laser Wavelength	λ	0.8 μm	0.8 μm	
Laser focal spot size	w_o	50 λ	50 λ	
Rayleigh Range	z_R	6.3 mm	6.3 mm	
Slippage Length	z_s	2.8 mm	2.8 mm	
Ideal Crossing Angle	θ	11.5 mrad	11.5 mrad	
Critical Energy	γ_c	68	68	(34 MeV)
Spot size on dielectric surface	w_1	51.3 λ	51.3 λ	
Fluence x time on dielectric surface	$F \cdot \Gamma_t$	2 J/cm^2	0.5 J/cm^2	
Laser Pulse Energy	E_γ	100 μJ	25 μJ	
Laser Pulse Length	Γ_t	100 fsec	5 psec	FWHM
Peak Electric Field	E_o	5.9 GV/m	0.42 GV/m	
Peak Axial Field	E_z	140 MV/m	9.8 MV/m	
Energy Gain	ΔW	290 keV	20 keV	Ideal phase particle
Electron Beam Energy Spread	Γ_E	20 keV	20 keV	FWHM

Production of High Brightness Beams for Laser Acceleration

The experiments of E163 share in common the need for an electron beam that has narrow energy spread and short bunch length. The energy spread must be kept low enough that the ±20 keV energy modulation induced by the laser fields is not masked either when it is present as an energy spread increase (as in Phase I), or when it is present as the acceleration or deceleration of the microbunches.

Transverse beam quality is less important, with the primary requirements being (1) the ability to produce a small spot (~10 x 20 μm) with reasonable beta functions, and (2) the attainment of a focus through the IFEL prebuncher that provides good coupling to the 800nm TEM_{00} mode. Available laser power puts the maximum reasonable transverse laser size in the IFEL prebuncher (and hence electron beam size) at 250 μm. For beta functions at the interaction point of ~5 mm, normalized emittances better than 2.4 x 9.6 π mm-mr are required.

The production of extremely low energy spread low charge bunches has been demonstrated at the DUVFEL facility at Brookhaven, with 20 pC bunches of 0.01% RMS energy spread[1] at 75 MeV (corresponding to 17.6 keV FWHM) having been routinely produced as part of their gun development program.

Using a gun that is identical in microwave design to the s-band gun at the Brookhaven ATF and DUVFEL facilities will allow E163 to draw on the extensive operational knowledge that has been amassed. This configuration is shown installed on the NLCTA beamline in Figure 1.

Short bunches may be produced in a straightforward manner from an rf gun because the photoemission process produces an electron pulse that has the same shape as the laser pulse. The strong electric fields in the rf gun violently accelerate the electron bunch, giving space charge forces less time to alter the electron bunch shape. The relaxed transverse emittances and reduced bunch charge afford additional latitude, allowing a large radius, short bunch (5 mm diameter, 0.8 ps FWHM pulse length) to be used, and for the launch phase to be early (30^o after zero-crossing), giving strong rf bunching in the gun. These parameters stand in marked contrast to operating parameters which optimize transverse emittance performance for a similar gun operated for a FEL: 1 nC, 2 mm diameter, 10 ps FWHM, and 50^o.

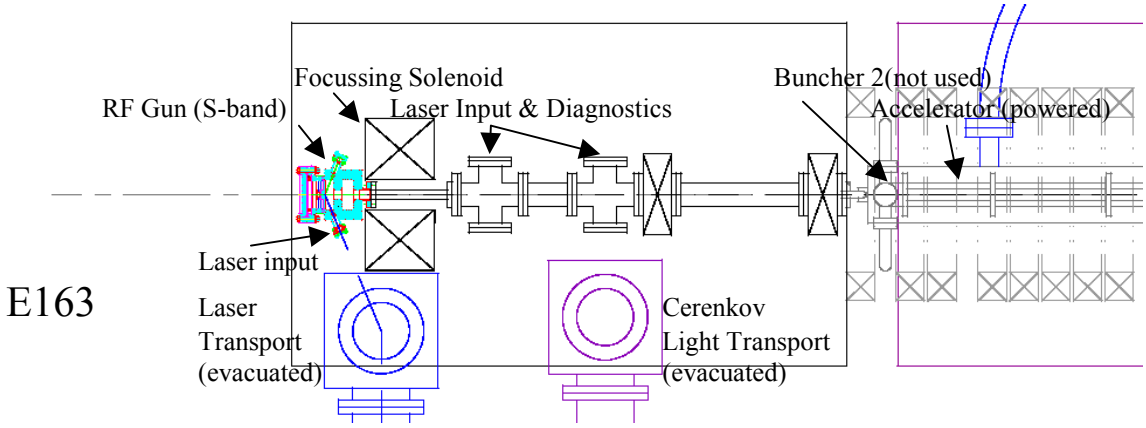

FIGURE 1. Rf gun shown installed at start of NLCTA beamline. The first and second crosses are to house the laser mirrors as well as various beam diagnostics. The ends of the vacuum light transport lines are also visible at the bottom of the figure.

The correlated energy spread and bunch length grow substantially in the long drift between the gun and x-band accelerator under strong space charge forces. This requires that one accelerating section be run slightly off-crest to remove the first-order correlation. The bunch is accelerated to 60 MeV in two 0.9 m long x-band accelerator sections and matched into the NLCTA chicane. Given that the x-band accelerator accounts for most of the beam's final energy, obtaining the required small energy spread means keeping the RMS bunch length to roughly $(\pi/2 - \sin^{-1}(1-\delta p/p_o))/\omega \sim$ 280 fsec for x-band frequencies and a momentum spread of $\delta p/p_o = 2\times10^{-4}$.

The chicane will be set to be isochronous, but it will still be dispersive at the midplane (η_x~20 cm), and with suitable adjustment of the chicane quads a very small horizontal beta function (β_x~4 mm) can be generated at this point, permitting very fine energy collimation of the beam. The NLCTA chicane has a collimator, profile screen, and wire scanner at this location for precisely this purpose.

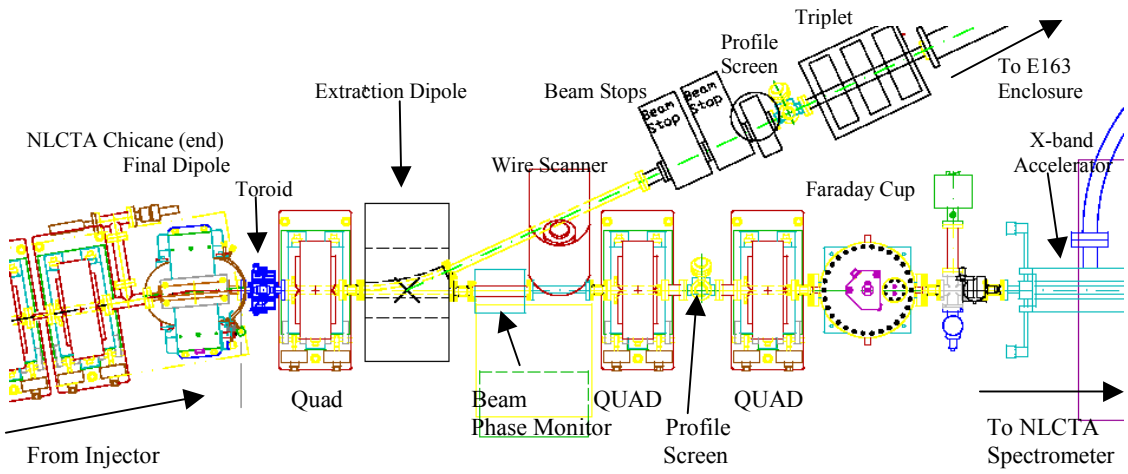

FIGURE 2. Extraction line for E163 shown installed immediately downstream of the NLCTA chicane.

The beam exits the NLCTA chicane, passes through a single matching quadrupole and then into the extraction dogleg leading to the E163 shielding enclosure. This arrangement is sketched in Figure 2. The dogleg is tuned to be first-order isochronous, with a pair of symmetrically placed quadrupole triplets being

used to invert the sign of the dispersion function and to provide focussing.

Matching between the dogleg and the final focus triplet will be accomplished within the E163 shielding enclosure using a quadrupole doublet. The layout within the E163 shielding enclosure is shown in Figure 3. A toroid at this location will provide a measure of the bunch charge as well as a means to reject those pulses that have lost too much charge on the beam collimator. The final focus triplet is positioned to allow fine focussing at the accelerator cell, both with and without the buncher IFEL.

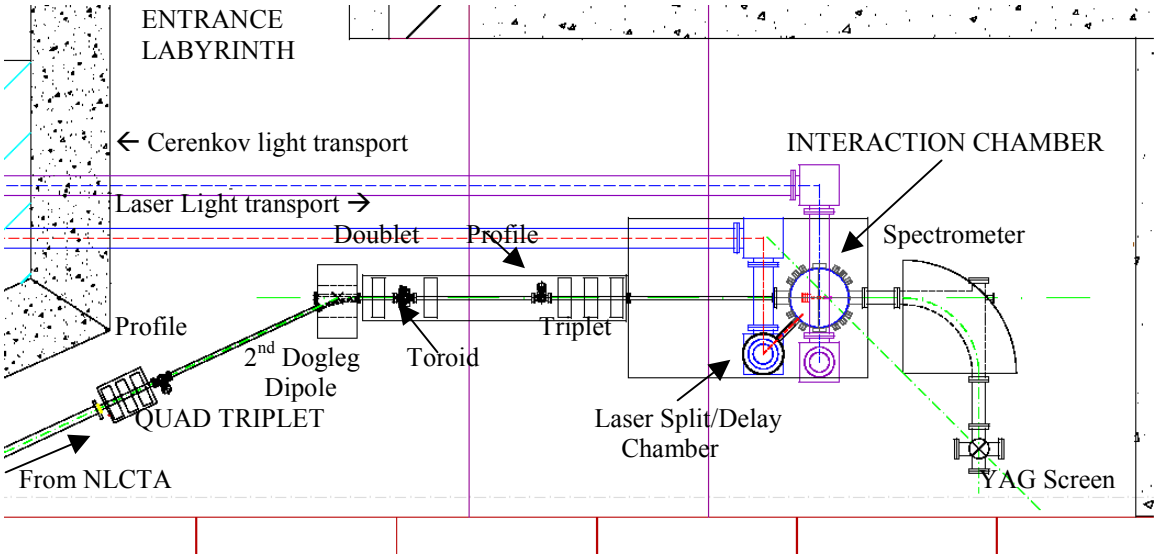

Figure 3. Layout of beamline and experiment components within the E163 shielding enclosure.

A quadrupole doublet and triplet provide flexible focussing for matching the beam into the laser accelerator cell. The laser accelerator cell, IFEL prebuncher and a short chicane are all housed within a common vacuum chamber called the interaction chamber. This arrangement is shown in Figure 3. As will be discussed below, the compactness of this arrangement is an essential feature for preserving the optical microbunching. A 90^{o} spectrometer and high resolution profile screen follow for precision spectrometry.

Causes and Cures for Drift

Two basic mechanisms of drift are considered here. The E163 experiment will be housed inside a concrete shielding enclosure that extends out of the eastern wall of End Station B, which has minimal environmental controls, and is therefore subject to considerable temperature variation. Thermal expansion of signal cables and the physical dimensions of certain key components therefore can introduce timing errors of various kinds through propagation time differences. In addition, the vibrations of equipment in and near End Station B could potentially also introduce timing errors through the movement of transport mirrors and the flexure of the mounting plate upon which the Phase II and Phase III laser acceleration experiments are performed.

The most demanding measurements currently envisioned in the E163 program call for taking continuous data sets composed of 4500 successive machine pulses. At 10 Hz, this requires the machine to be stable for approximately 8 minutes.

For all E163 experiments, thermal phase shifts in the generation and transport of the three basic frequencies (79 1/3 MHz for the laser, 2856 MHz for the gun, and 11424 MHz for the linac) will comprise the dominant source of timing errors between the electron and laser pulses. The basic stability requirement at this level is that timing shifts of no more than the laser pulse duration (5.0 psec FWHM) should occur over

a 5 minute time interval or the laser and electron pulses will fall out of overlap. The use of thermally insulated, temperature-controlled, low thermal coefficient Heliax cables for distributing these signals will be essential. With similar measures, a 5-minute timing drift of less than 80 fsec has been demonstrated in the rf distribution cabling of the damping rings at SLAC.

In Phase II and Phase III, there is the added constraint that the IFEL prebuncher and accelerator should remain properly phased at the optical time scale. The basic stability requirement at this level is that timing shifts of no more than 0.2 fsec (corresponding to $\lambda/10$) should occur over a 5 minute time interval. This restriction applies only to the laser and electron path lengths between the IFEL prebuncher and laser accelerator cell. The use of ultra low thermal expansion materials (e.g. a Zerodur mounting plate), active temperature control, and the minimization of path lengths are all key to minimizing thermal drifts. The use of rigid, massive mounts for optical components and vibration-absorbing materials in the support for the interaction chamber itself will be needed to ensure mechanical vibration of optical components does not cause path length variations.

Analysis of Jitter

The three dominant jitter sources that will influence the E163 experiments are (1) laser intensity jitter, leading to bunch charge jitter, (2) phase jitter of the rf structures, leading to both timing and energy jitter, and (3) accelerating voltage amplitude jitter of the rf structures, leading to energy jitter. For the very low charge and low peak current bunches considered here, the charge jitter is essentially benign. Timing and energy jitters are closely coupled to beam qualities important to the experiments, however, and have serious impact.

In this section, we will make simple estimates of the couplings between the dominant jitter sources and the parameters of experimental interest. Detailed Monte Carlo simulations of machine performance with jitter are presented in the next section.

Feed through of jitter into transverse beam properties (emittance, spot centroid) has little effect on the E163 experiments as the emittance requirements are not demanding, and the large beam demagnification ($\sqrt{\overline{\beta} / \beta^*} \approx 310$) from the final focus triplet highly suppresses centroid motion.

The introduction of an energy collimator with a restrictive aperture in the NLCTA chicane not only serves to improve the energy spread but plays an important role in limiting the effects that jitters in the injector will have on the experiment.

First, the collimator defines a specific, fixed range of beam energy that can be transmitted to the experiment hence the energy centroid jitter of the transmitted beam will be reduced. Second, since the gun and accelerator sections are run off crest, bunches that are off-phase will in general also be off-energy, and hence the collimator will give some reduction in the timing jitter as well. Third, bunches which are off-energy because they are off-phase generally have larger energy spreads, and hence the collimator will give some reduction in the component of the energy spread jitter which derives from rf phase jitter.

For E163, there are 4 unique jitter parameters in the rf system: the phase and amplitude of the s-band klystron output (driving the gun) and the phase and amplitude of the x-band klystron that drives both 0.9 m accelerator structures. As only the relative phase of the s- and x-band sources with respect to the laser timing is relevant, the laser timing is taken as the absolute reference.

A quick way to understand the collimator's impact on jitter feed through is to compute its acceptance as a function of the jittering parameters . The beam energy, in rough approximation, is given by:

$$E = E_{gun}\sin(\phi_{gun}) + E_{A1}\sin(\omega T_{G1} + \phi_{A1}) + E_{A2}\sin(\omega(T_{G1} + T_{12}) + \phi_{A2})$$

where values for the gun and linac energy gains are E_{gun}=5 MeV, E_{A1}= E_{A2}=27.5 MeV, the mean phase of the electron bunch w.r.t. the rf wave in the gun is ϕ_{gun}=66.5^o (computed with Parmela), the linacs are phased at ϕ_{A1}= ϕ_{A2}=90.6^o, ω is the x-band rf angular frequency, and T_{G1} and T_{12} are the transit times between the gun and accelerator 1, and between accelerators 1 and 2, respectively.

Figure 4 below shows two contour plots of the beam energy (actually, one as a function of gun and linac phase (at constant amplitudes), and one as a function of gun and linac amplitude (at constant phases). The design energy contour and contours ±15 keV and ±30 keV away from the reference contour are shown to indicate the edges of the collimator aperture. Dotted lines have been overplayed to indicate the measured values for the phase and amplitude jitter of the NLCTA x-band accelerator. It is clear from the figures that the linac amplitude jitter is the more serious issue, and will lead to the largest number of shots that will be rejected by the collimator.

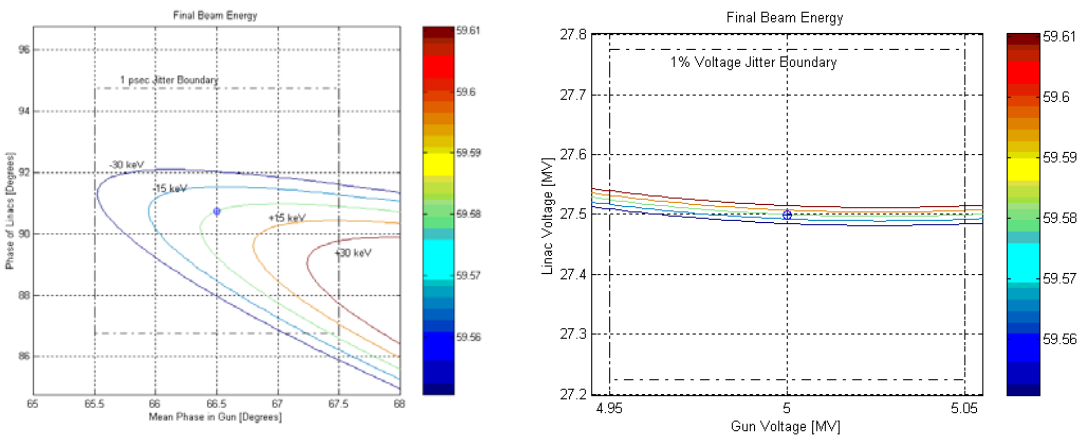

FIGURE 4: (Left) Region of gun and linac phase allowed by energy collimator. (Right) Region of gun and linac voltage allowed by energy collimator. The central (green) contour corresponds to the central momentum accepted by the collimator, the remaining contours show acceptance of ±15 keV and ±30 keV. The dotted box indicates the 1 picosecond (left) and 1% (right) RMS jitter boundaries. The color scale indicates beam energy in MeV.

The gun and linac phases in the case shown in Figure 4 above have been optimized to produce an electron bunch with no first-order phase/energy correlation. This case gives the maximum transmitted charge through the NLCTA collimator slits for the ideal beam, but because the beam energy spread is comparable to the collimator acceptance, strongly converts momentum jitter into charge jitter. The end result is infrequent, high charge (~30 pC) bunches with good momentum spread.

An alternate and more desirable strategy is to deliberately induce a phase/energy correlation on the beam, giving a momentum spread that is larger than the acceptance of the collimator. By "painting" the collimator slit with a larger energy spread beam, the transmitted fraction is small, but the conversion of momentum jitter into charge jitter is reduced. In addition, running the linac off-crest to achieve this condition also strongly correlates time and momentum, allowing some temporal collimation as well. The end result is frequent, low charge (2-5 pC) bunches with good momentum spread. This case will be referred to as "painting", and is calculated and displayed in the sample Phase I and Phase II run data in the following sections.

The energy jitter also contributes a timing jitter between the electron and laser pulses at the accelerator cell from straightforward time-of-flight effects since the chicane and dogleg are first-order isochronous. The time of flight variation is:

$$\frac{1}{m_e c^2}\frac{dt}{d\gamma} = \frac{1}{m_e c^2}\frac{d}{d\gamma}\int\frac{ds}{c\beta(s)} \approx \frac{L}{c}\left[\frac{1}{\sqrt{\gamma^2-1}} - \frac{\gamma^2}{(\gamma^2-1)^{3/2}}\right]\frac{1}{m_e c^2} \approx -0.07\ \text{ps/m}_e\text{c}^2$$

with L~35 meters being the path length between the RF device causing the energy jitter and the laser accelerator cell. The approximate form is reasonable as $\beta \rightarrow 0.9$ just 7.5 mm after emission from the cathode. The collimator will be set to have an energy acceptance of approximately $2\text{x}10^{-4}$, which implies that the temporal jitter (due to time-of-flight effects) will be limited to $\delta t \approx \gamma(\delta\gamma/\gamma_o)(dt/d\gamma) \approx 0.66$ psec full-width, or 0.19 psec RMS, if the energy jitter present at the collimator is approximately uniform in distribution. The introduction of the collimator serves not only to produce beams of narrower energy spread, but also to help suppress timing and energy jitter.

Numerical Model

A fully three-dimensional simulation capable of modeling RF gun performance, acceleration, coherent synchrotron radiation effects in the chicane and dogleg dipoles, wakefield effects in the energy collimator, the IFEL interaction in the prebuncher, the subsequent bunching and acceleration, and finally the downstream spectrometer performance is required to quantify the effects that will significantly contribute to the beam quality either intrinsically (e.g. wakefield effects), or through jitter (e.g. phase jitter in the RF structures). A 3D model has been assembled from three distinct codes sharing information via 6-D phase space exchange. Initial magnet settings for the chicane, dogleg, and final focus magnets were calculated in Transport, using the present chicane configuration of the NLCTA[2] as a starting point. These magnet settings were then used as the starting point for optimization using Elegant.

Simulation of the full beamline was done using phase space input from Parmela for the gun and low energy acceleration section and at no point relied on representing the very non-thermal, non-Gaussian distributions of the electron bunch by a Twiss parameterization. The laser acceleration interaction was modeled in a separate step, using a Matlab program written for the purpose. For the Phase II experiment Genesis was used to model the IFEL interaction, and Elegant used to model the bunching process through the final chicane into the laser accelerator cell. After the laser interaction, Elegant was again used to finish propagation to the spectrometer focal plane, where distributions were recorded, just as will be the case with the real experiment. Wakefield effects are treated in a perturbative manner in Elegant using monopole wakefield Green functions calculated by mode summation techniques[3] and checked by Xwake. Figure 5 summarizes the computational model.

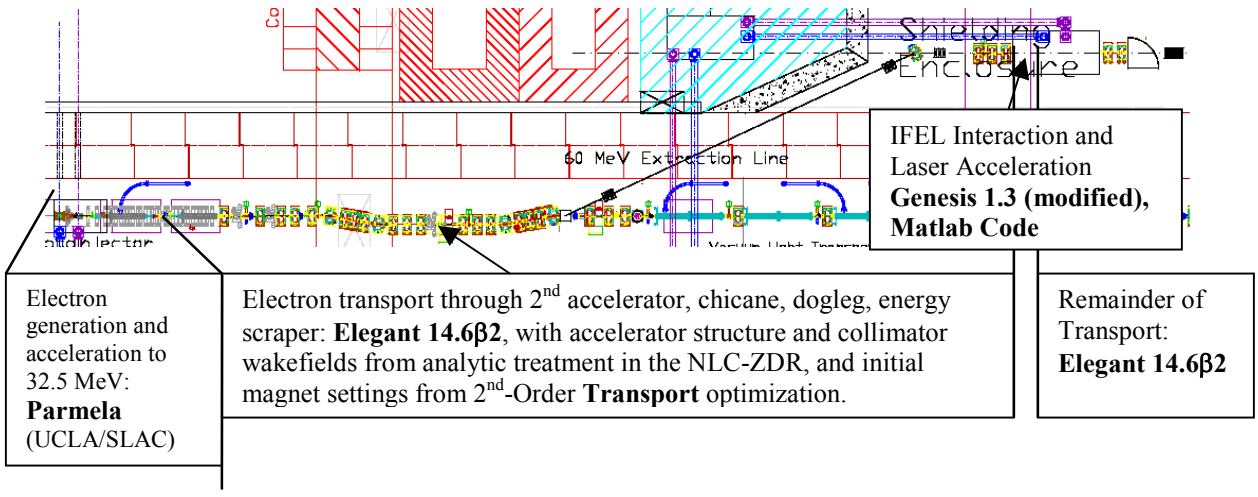

FIGURE 5. Computation codes used for modeling each section of the NLCTA and the E163 experiment.

Parmela is a 3D tracking code with space charge forces, mapped RF fields and second-order bending and focussing elements, and is suitable for modeling the electron emission and preacceleration process. Parmela's non-symplectic integrator makes it unsuitable for simulating long beamlines, however. In addition, Parmela does not include wakefield effects (except at the photocathode) or the effects of coherent or incoherent synchrotron radiation effects in bends.

Elegant is a 3D tracking code with no space charge forces, simplified representation of RF fields, second-order or numerically integrated focussing and bending elements, and an approximate method for calculating incoherent and coherent synchrotron radiation losses and their effects on the beam quality. Wakefields may be approximated by kicking the beam with a user-input Green function calculated by a wakefield code. The lack of space-charge forces makes Elegant unsuitable for modeling the electron gun and first accelerator section.

Genesis is a 2+1D numerical integration FEL code that solves the longitudinal differential equations for a beam interacting with a radiation field in the presence of a wiggler, and calculates the transverse dynamics with a matrix treatment. The lack of standard focussing and bending elements makes this code unsuitable for simulating anything but the IFEL prebunching dynamics. This version of Genesis has been modified to correctly model the interaction of a bunched electron beam with a finite length laser pulse. It has also been modified to read and write Elegant-compatible phase space files.

Matlab is a general purpose plotting and analysis program. It is used in these simulations two ways: first to drive the succession of simulation codes to make the simulated data for the "time scans" of Phase I and "phase scans" of Phase II, and second to compute the electron beam interaction with the laser fields in the accelerator cell.

Cross-Check of the Model

As a check of this model a Parmela simulation was made of the entire E163 beamline to establish the influence of space charge, and is shown in Figure 6. Beyond the first 0.9 m x-band accelerator section there is only slight broadening of the energy spread due to space charge, and thus switching to Elegant (which does not include space charge effects) at this point introduces little error. Beamline dimensions, quadrupole, and dipole strengths used in the Parmela simulation are transferred without correction or retuning from the Elegant simulation, with one exception. The betatron phase advance error (induced by the slight space charge tune depression) is partially compensated using the matching quad between the chicane and dogleg to restore reasonable beta functions in the dogleg.

That the two different codes give quite similar results establishes that the space charge effects (modeled only in Parmela), wakefield and CSR effects (modeled only in Elegant) do not appreciably contribute to the beam dynamics. The slowly accruing betatron phase error seen in the Parmela simulations is the most visible effect of space charge, and can be easily compensated by a slight increase in quad strengths.

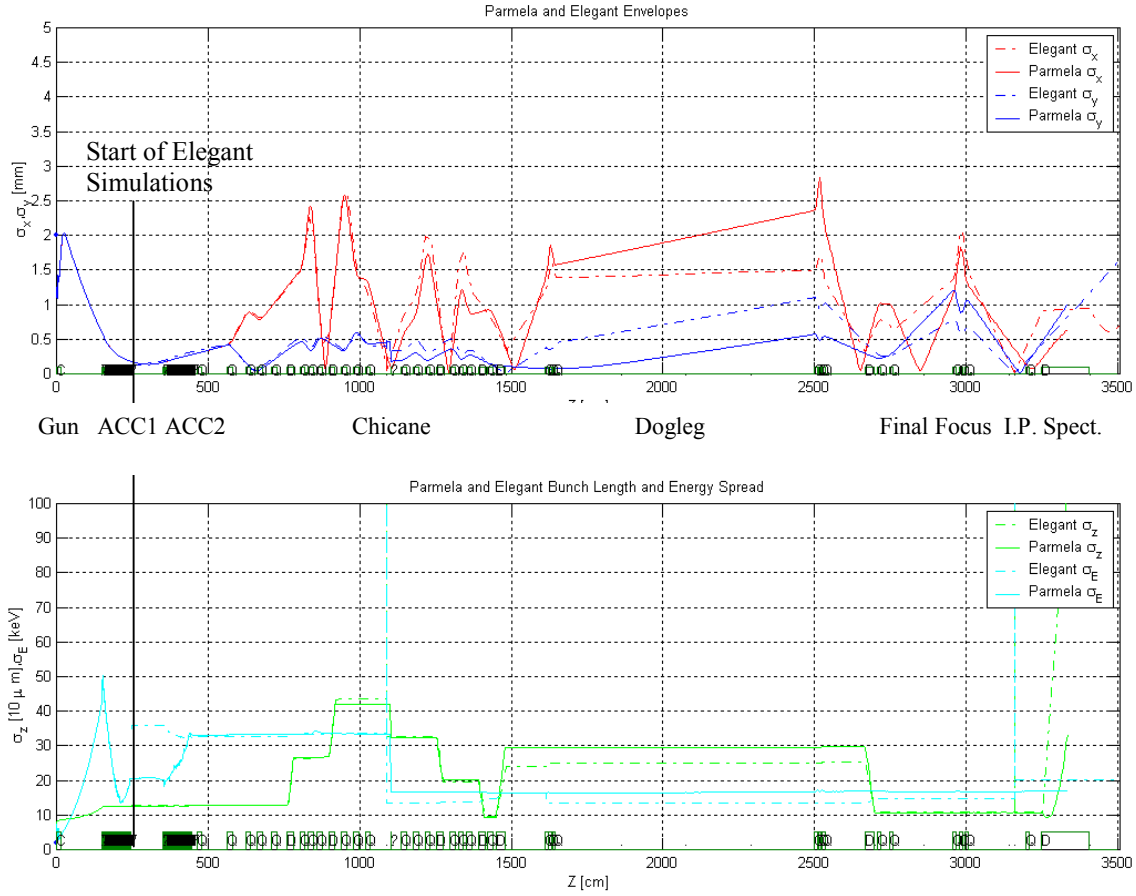

FIGURE 6: Parmela and Elegant simulations of entire E163 beamline. Horizontal and Vertical envelopes (top) and bunch length and energy spread (bottom) are displayed.

The short bunch length (corresponding to 19 A peak current) will cause an increase in the energy spread of the bunch in the gun, x-band linac, at the NLCTA collimator, and via coherent synchrotron radiation (CSR) in the bends. The wakefield effect of the gun is negligible in comparison to the effect of the x-band linacs because it has fewer irises (2 vs. 105) that are much further from the beam (12.5 mm vs. 3.9 mm). Consequently, the wakefield effects in the gun have been neglected. The monopole wake for a single cell of the x-band was computed using mode summation techniques for the NLC structures. The monopole wake for the collimator was approximated by scaling the NLC single-cell wake using Gluckstern's[4] expression for the monopole Green function at infinite frequency.

Wakefield effects from the x-band accelerator sections and the collimator are shown in Figure 7. In each case the longitudinal phase space is displayed with and without wakefield effects included. The effects of dispersion in the NLCTA chicane are plainly visible in the longitudinal phase space at the collimator. The x-band accelerator contributes significantly, and has to be corrected by adjusting the linac phase slightly to compensate. The collimator, although 8 times closer to the beam than the x-band structure irises, is applied to the beam while it is significantly lengthened (by more than a factor of 3) in the dispersive section of the compressor, resulting in somewhat reduced wakefield effect.

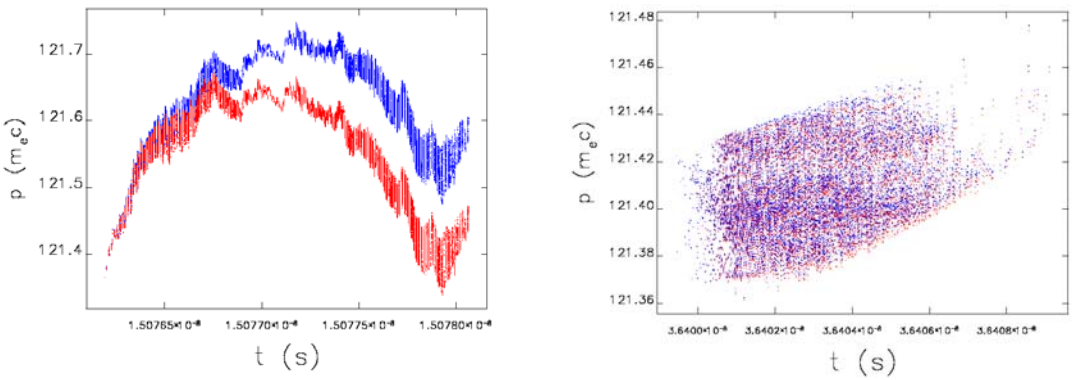

FIGURE 7. Wakefield effects on 50 pC bunch from the x-band accelerating structures (left) and collimator at center of NLCTA chicane (right). Red: wakefield effect applied, blue: no wakefield effect applied.

Elegant was used to calculate the effects of CSR in the NLCTA chicane, the extraction dogleg, the IFEL wiggler, and final spectrometer. As charge scraping occurs at the laser interaction cell, thereby reducing CSR effects in the spectrometer, the most dramatic impact comes from the 25° bend magnets of the extraction dogleg, and the results are displayed in Figure 8 below. By contrast, the short length (3 periods)

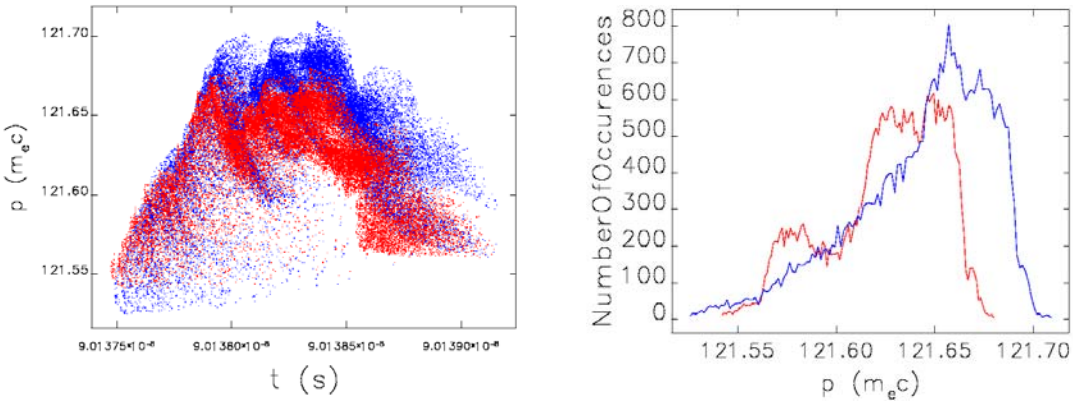

FIGURE 8. Effects of coherent synchrotron radiation on the longitudinal phase space in the 25° dogleg bend pair, for a 30 pC, 1 psec FWHM bunch. Left: phase space, right: momentum histograms. Red: CSR applied, blue: no CSR effects included.

and small beam deflection (0.8°) in the IFEL wiggler cause no calculable beam degradation.

The laser/electron beam interaction was modeled as a simple point transformation by kicking each electron according to its position in time and transverse position at the accelerator cell according to:

$$\Delta\gamma = \frac{V_o}{m_e c^2}\exp\left(-\frac{r^2}{w_o^{\,2}}\right)\exp\left(-\frac{(t-T)^2}{2\sigma_t}\right)\sin((t-T)\omega)$$

with V_o=20 kV being the peak laser interaction kick, calculated using equation (6) in reference [5], w_o=40 μm being the Gaussian beam waist parameter, t being the time the electron reaches the accelerator cell, T=105.496 nsec being the time (measured from the instant the UV laser pulse strikes the photocathode) the laser pulse arrives at the accelerator cell, σ_t=2.1 psec being the laser pulse length, and $\omega=2\pi c/\lambda$, with λ=0.8 μm.

Phases II and III of E163 will require the staging of an IFEL prebuncher and a laser accelerator. The optical microbunches formed in the IFEL can be easily washed out by path length differences, necessitating careful beam transport of the bunched beam. Changes in the beam trajectory once the optical energy modulation has been "imprinted" by the IFEL very easily can lead to washout of the bunching. Consequently, the IFEL is positioned after the final focus optics as close as possible to the laser accelerator cell. A short (10 cm overall length), low bend-angle (3.4°) magnetic chicane is used to convert the small energy modulation from the IFEL into spatial bunching. As path length differences of only ~800 nm are needed between particles with energies differing by $\delta p/p_o \sim 10^{-3}$, the chicane need only produce a temporal dispersion of $(\phi|\delta p/p_o)=R_{56}=0.8$ mm. The shallow angles of the bends of the chicane, together with a balancing of the focusing strength in each plane, ensure that the chicane does not appreciably alter the transverse trajectories, which would compromise the bunching, which is displayed in Figure 9. This plot shows the bunching parameter $B=I_1/(2I_0)$, where I_1 is the amplitude of the Fourier component of the current at the optical wavelength, and I_0 is the amplitude of the "DC" component, as computed with Elegant and Genesis.

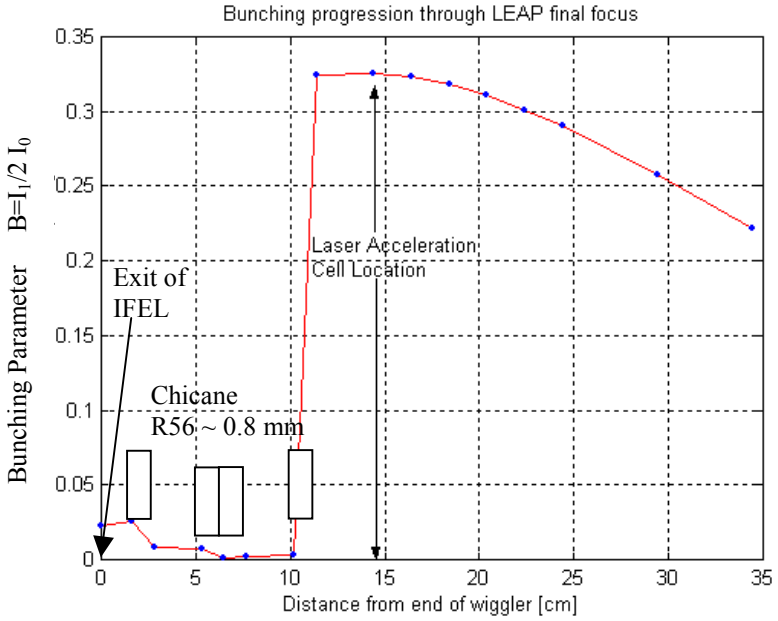

FIGURE 9. Bunching evolution starting from the exit of the IFEL prebuncher, and proceeding through the chicane, the laser acceleration cell (not powered for this calculation), and a drift.

The small acceleration available in the phase II single accelerator cell makes it important to accomplish bunching without inducing a large energy spread (correlated or not) that will make observing the accelerated bunch difficult. Consequently, a short IFEL (3 periods only) optimized to couple 800nm radiation to the 60 MeV electron beam will be used. The required wiggler has modest strength (a_w=0.455) and a reasonable period at 1.8 cm.

These elements were combined to make an end-to-end simulation model, using Parmela to model beam production at the photocathode and propagation to the exit of the first accelerator, Elegant to model the remainder of the beamline to the laser accelerator cell (including wakefield and CSR effects), Matlab to model the laser interaction, and Elegant to model the remaining transport through the spectrometer to the profile screen. For phase II, the added IFEL prebunching process was modeled using Genesis.

As the Parmela portion of the simulation requires ~4 hours, a set of 81 Parmela simulations covering gun phase errors from –1 psec to +1 psec and first accelerator section phase errors from –1 psec to +1 psec was made, and the final phase spaces stored in a library. Random phases and amplitudes were selected from

Gaussian distributions, then used to (1) select the correct Parmela phase space to load, and (2) choose the parameters in the Elegant simulation. Amplitude errors in the gun are accounted for by shifting the launch phase to give an equivalent beam energy error. Amplitude errors in the first accelerating section are accounted for by doubling the amplitude error of the second accelerator section. (n.b., the first a second accelerator sections are driven by a common klystron, so the phase and amplitude errors do add coherently).

Beam Collimation

The collimator in the NLCTA chicane functions not only to reduce the beam energy spread, but to reduce the jitter in the first and second moments of the beam time and energy distributions. Figure 10 below shows the results of a Monte Carlo calculation of the effect the collimator will have on these beam qualities. Using 1 ps RMS phase jitter, 1% rf amplitude jitter, and 5% charge jitter, all normally distributed, 20000 bunches were generated and passed through the collimator to compute transmission probability as a function of the beam properties. The discrete banding in the time coordinate is a direct result of using the discrete library of initial phase spaces for the gun and first accelerator section.

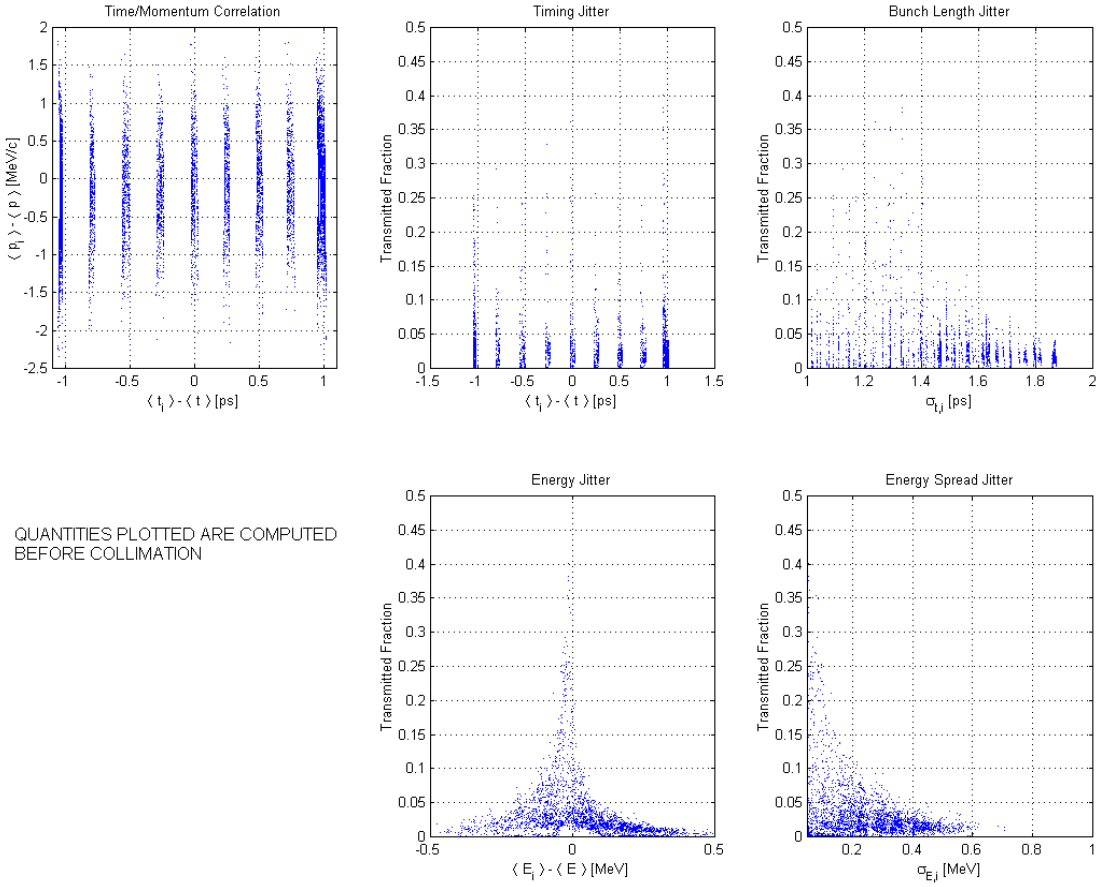

FIGURE 10. Monte Carlo simulation of beam transmission through the NLCTA collimator for the "painting" case. All beam properties shown are computed for the bunch prior to collimation. Index *i* refers to a specific microbunch.

The time-momentum correlation plot illustrates how well the collimator may be expected to reject timing jitter from the gun and linac. The gradual upward slope from one band to the next is a result of running off-crest in the s-band gun. The steep downward slope within each band is a result of running off-crest in the x-band linac. Since the linac voltage is 11 times the gun voltage, and the linac frequency is 4 times the gun

frequency, the linac temporal jitter is much more strongly converted into energy jitter and will be well rejected by the collimator. The gun timing jitter, conversely, is quite poorly rejected and feeds through.

The bunch energy spread and bunch length are both reduced by the collimator, as is seen in the two plots of beam transmission on the right in Figure 10. For example, by measuring the post-collimator bunch charge and rejecting pulses with less than 5% charge transmission (0.05 on the plot scale), narrower bunches in time and energy are selected out the larger distribution.

It is clear from Figure 10 that the collimator serves to reduce the jitter in the mean energy, the energy spread, and the bunch length. It is also clear from the time-momentum correlation plot that the collimator will reduce feed through of phase jitter from the x-band accelerator, which imparts a strong time-energy correlation, but will not give much temporal jitter reduction for the gun.

Given that typical operation involves 50 pC, 60 MeV bunches striking the collimator at 10 Hz, the average power dissipation is trivial at less than 30 mW CW, assuming the beam is stopped within the collimator. The energy deposited per unit area and instantaneous temperature rise of a 2 mm thick tungsten collimator are also trivial at 2.3 J/cm^2 and 4.5 ^{o}C, respectively, for the computed spot size of σ_x x σ_y = 47 x 65 μm.

Dark Current

Because the photoemitted beam has little charge, it is important to estimate the impact of dark current on diagnostics. Figure 11 shows that the dark current is rapidly lost in the NLCTA beamline. The plot was generated assuming an average dark current of 1 mA is detectable immediately after the gun, and shows the per-rf-bucket dark current charge that is transmitted through the beamline. The dark current is presumed to be emitted entirely from a 2 cm diameter region on the cathode in the ±10 degree RMS phase range about the rf voltage crest, as would approximately be the case for field emission. Charge emitted from the first iris is neglected as it has significantly lower energy and is lost very early in the transport. During an rf pulse lasting 6 μsec, there are ~1.7x10^4 rf buckets, giving an integrated charge (per rf pulse) on screens following the gun of ~7 nC. Screens following the second linac section will see an integrated charge of ~8 pC, and screens following the NLCTA collimator will see negligible integrated dark current.

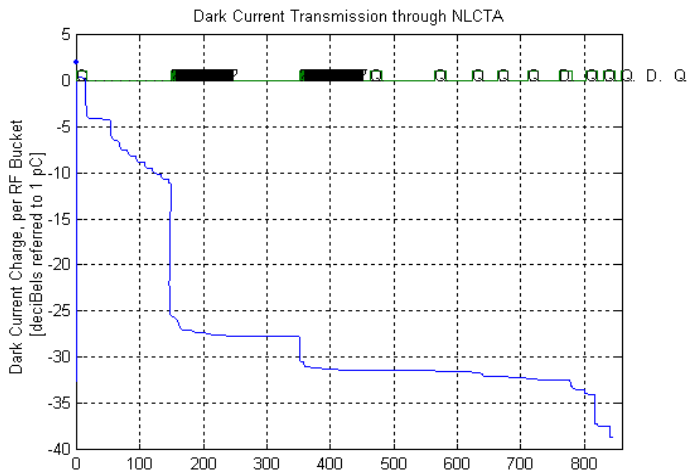

FIGURE 11. Dark current transmission through the NLCTA beamline, shown on a logarithmic scale, referenced to 1 pC per rf bucket.

Beam diagnosis immediately after the gun will likely require that the bunch charge be increased to get a clear signal. With tuning completed, the bunch charge can then be decreased to the operating value. Methods for scaling the bunch charge in a manner that maintains the beam dynamics without the need to change magnet settings are well documented[6]. Beam diagnosis downstream of the x-band linacs will not be

a problem as the dark current is reduced by more than three orders of magnitude at this location. Beyond the narrow acceptance NLCTA collimator, there is negligible dark current transmission.

Simulation of a Phase I Time Scan

The most demanding measurement envisioned for Phase I, in terms of machine stability and complexity of the measurement, is the timing scan performed to establish the time relationship between the electron and laser bunches at the laser acceleration cell. Streak-camera based timing alignment leaves an uncertainty of ±5 psec in the absolute timing of the electron and laser pulses, and requires that a search be performed within this uncertainty window. The overlap condition is sought by scanning the laser timing until the energy modulation signature is seen. With a 5 psec laser pulse and a 1 psec long electron bunch, the 10 psec must be scanned in steps smaller than a picosecond to have a good chance of observing the signature.

The numerical model described above was run repeatedly in Monte Carlo fashion, selecting gun and linac phases from a Gaussian distribution with 1 psec RMS width, selecting rf amplitudes from a Gaussian distribution with a 1% RMS width, and selecting beam charges from a Gaussian distribution with a 5% RMS width. This case illustrates "painting" collimation, with bunches with less than 5% of the initial bunch charge being rejected and the data point re-acquired.

The "time scan" modeled here is a scan of the timing between the electron and laser pulses from –5 psec to +5 psec in 0.05 psec steps, with optimum overlap occurring at 0 psec (image #101). This requires 200 valid machine shots, which given the 4.5% probability that a beam survives the collimator, requires roughly 4500 machine shots. Running at 10 Hz, a single data set would take less than 8 minutes to acquire.

Histograms of the beam's horizontal coordinate at imaging plane of the spectrometer were made to establish the energy spectrum as it would be recorded by the profile screen. This folds in the resolution of the spectrometer. Region of view and histogram binning were chosen to match the 1 cm field of view and 1024 pixel ICCD camera used to record the spectra.

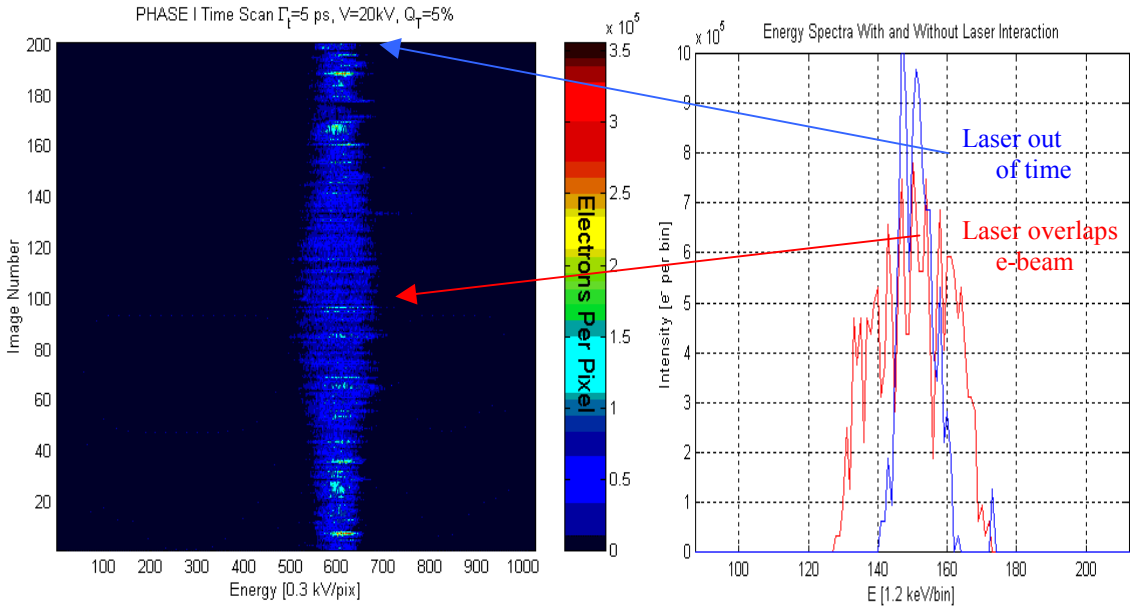

FIGURE 12. Simulated time scan data set (left), and comparison energy profiles for laser at full overlap (red) and out of time (blue), on an expanded scale. The relative timing between laser and electron bunch is swept from –5 psec to +5psec, with optimum overlap occurring at 0 psec (image #101). The laser pulse length is 5.0 ps FWHM, the laser-induced energy modulation amplitude is ±20 kV.

These spectra are displayed in Figure 12 below. The horizontal coordinate is the energy of the beam, the vertical coordinate is the data point (image) number. Image 1 corresponds to the laser being 5 psec early; image 101 corresponds to the laser being exactly overlapped with the electron pulse; image 200 corresponds to the laser being 5 psec late.

Simple data analysis makes the broadening clear. Figure 13 is effectively a contour plot of charge density, plotted against energy on the horizontal axis, and laser timing on the vertical axis. The contours are drawn at 80%, 66%, 33%, 25%, and 15% of the maximum value in each profile.

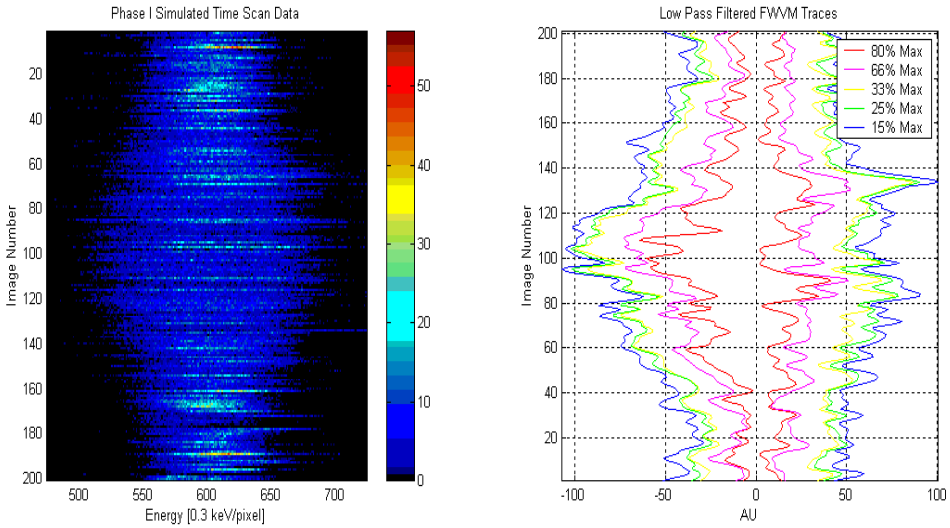

FIGURE 13. Expanded view of raw data (left) and half-width-at-specified-value traces (right) for the energy spectra sequence shown in Figure 12 above. The energy width broadening due to the laser interaction is plainly visible on the sharply rising high-energy side of the distribution. Note horizontal scales are magnified compared to Figure 12.

The broadening induced by the laser interaction is plainly visible on both the high and low energy sides of the distribution. Another effect of painting the momentum collimator slits is to produce outgoing beam with well defined upper and lower energy bounds on each shot, giving rise to well defined edges (see Figure 14 below) on the energy profiles. The laser interaction pushes electrons beyond this well defined energy edge, making the interaction easy to see, despite the jitter.

In phases II and III, this same time scan technique will be used twice in succession to establish that the electron beam is timed to the laser pulse in the IFEL and to the laser pulse in the accelerator cell. Once the overlap timing condition is established, an optical phase scan is possible to observe the dependence of the energy of the optically captured beam on the relative phase between the IFEL prebuncher and laser accelerator.

Simulation of a Null Interaction Data Set

For reference, a set of 200 images calculated as above are shown in Figure 14 with no laser interaction at all, both with and without collimation and charge thresholding. This gives a sense of the machine jitter present at the experiment itself, and of the effects that painting collimation and rejection of shots with insufficient charge have on the quality of the probe electron beam. Collimation gives rise to sharply defined edges to the energy distribution, while charge thresholding ensures that data is acquired only when there is sufficient charge in the probe beam to make a valid measurement.

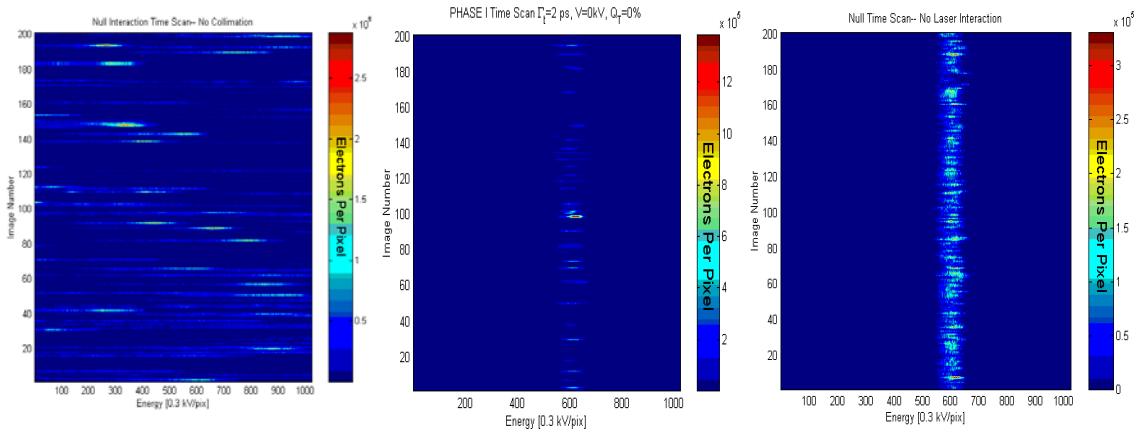

FIGURE 14. Null interaction time scan data sets: (left) with no collimation or charge thresholding, (center) with collimation only, and (right) with collimation and thresholding. Note that intensity per pixel has decreased an order of magnitude, but probe electron bunch has well defined energy characteristics. Bunch parameters and jitter are as in figures 12 and 13 above, but no laser interaction is present.

Simulation of a Phase II Phase Scan

The most demanding measurement envisioned for Phase II and Phase III experiments is the optical phase scan, used to establish the acceleration gradient and fraction of beam trapped by the optical bunching and accelerating processes. In this case, the relative optical phase of the IFEL and laser accelerator cell are varied over a full optical cycle in small steps. Figure 15 below shows a phase scan under the ideal conditions of no jitter or drift, together with a plot of the centroid energy of the entire electron population (optically trapped or not, optically accelerated or not). As with the time scan, the image displays a sequence of histograms of the beam energy, as registered by the profile screen after the spectrometer. The relative phase between the IFEL prebuncher and laser accelerator is varied in 10 degree steps with each successive image. This case illustrates "scraping" collimation, with bunches with less than 25% of the initial bunch charge being rejected and the data point re-acquired. The displayed scan would require little more than a minute of stable machine operation to acquire.

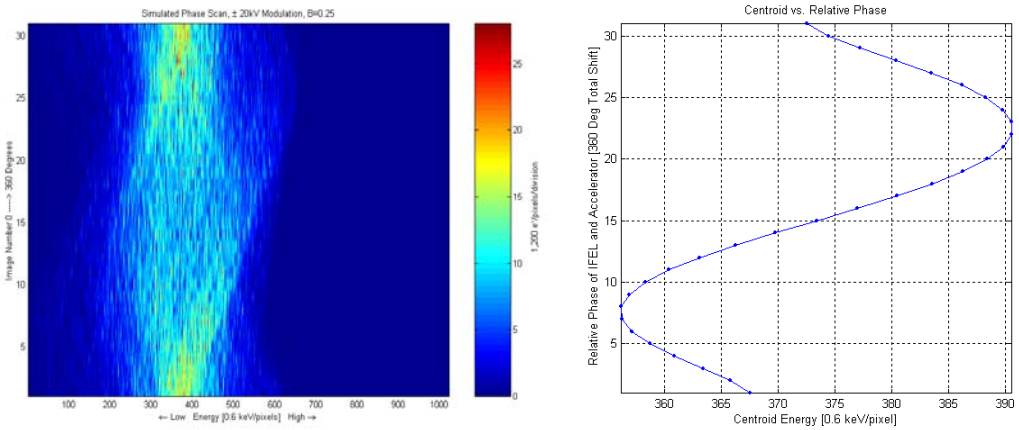

FIGURE 15. Simulated phase scan (left), showing measured energy spectra as a function of the relative optical phase of the buncher and accelerator, and centroid energy (right, on magnified horizontal scale). Accelerating phase occurs at 0 degrees. The peak energy gain in the laser accelerator is 20 kV. No jitters are present in this calculation. Despite the relatively poor bunching, the observable centroid movement (of all electrons, whether bunched in the correct phase and not) is ±10 keV.

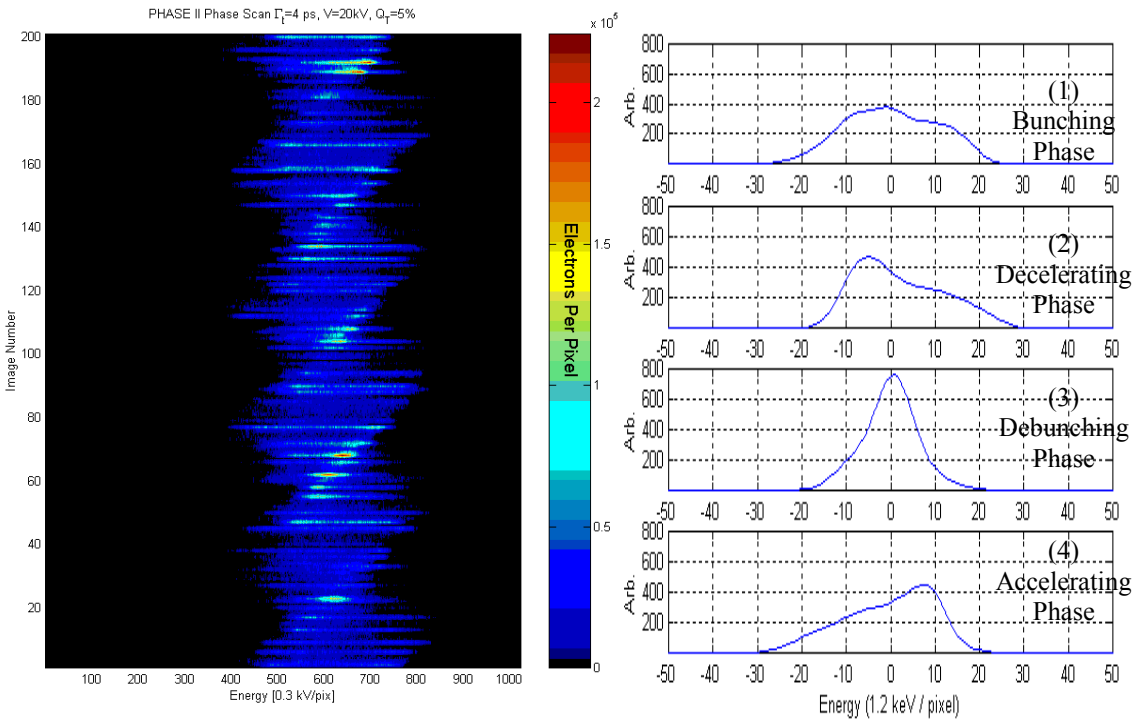

FIGURE 16. Simulated phase scan with jitter added (left), covering 5 optical cycles of variation in the relative phase between IFEL and laser accelerator, and averaged spectra (right) at (1) bunching, (2) decelerating, (3) debunching, and (4) accelerating phase.

Individual energy profiles have been shown at four distinct phases by averaging together profiles taken at the same relative optical phase between the IFEL prebuncher and laser accelerator. A simple statistic constructed from the ratio of the peak height of the energy profile to the width of the profile gives a clear indication of the 5 full optical cycle variation in phase between the IFEL prebuncher and accelerator cell and is shown in Figure 17 below.

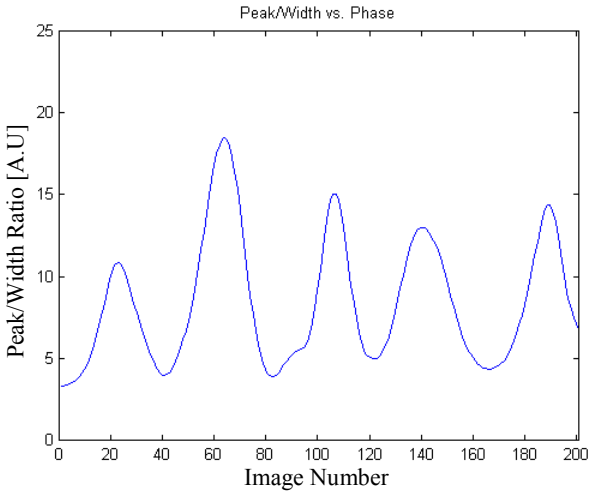

FIGURE 17. Plot of height/width ratio (a measure of energy spread) for the sequence of images shown in Figure 16. The 5 full cycles of phase variation are visible as five full cycles of variation in this statistic.

Operation of the NLCTA at 1 nC

Ongoing experiments in RF breakdown at the NLCTA call for a 1 nC electron bunch to be propagated through the downstream accelerating sections and into the NLCTA spectrometer. There must be sufficient current to excite the fundamental mode of the structure to permit a shunt impedance estimation for the structure, which allows estimation of the RF damage to the structure. Simulations of the modified NLCTA to demonstrate generation and transport of a 1 nC, 1.4 ps RMS bunch (current: 285 amps) through the downstream accelerating structures and into the spectrometer is shown in Figures 18, 19, and 20 below.

Figure 18 is a Parmela simulation of the gun and first accelerator section, with laser parameters and solenoid settings chosen to give 1 nC bunches of good quality. The air-core solenoid enclosing the x-band accelerating sections is powered in this case, unlike to the 50 pC cases shown earlier. The laser pulse length is 1.4 ps FWHM, and the radius is 1.0 mm, with the launch angle maintained at 30°. As with the 50 pC case, the laser pulse length and electron bunch length are much shorter than for the "usual" case (BNL-ATF/UCLA/GTF/ANL-LEUTL, etc.) and correspondingly, the transverse emittances are larger.

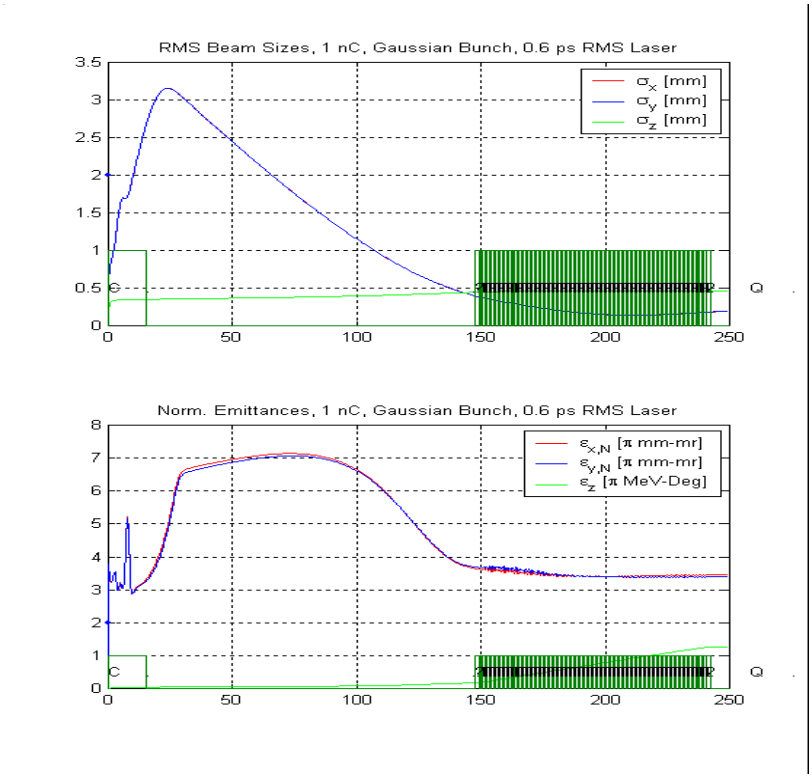

FIGURE 18. Parmela simulation of 1 nC bunch evolution through the s-band photoinjector and first 0.9 m x-band accelerator section of the E163 beamline. Top: RMS bunch sizes in millimeters, bottom: normalized transverse and longitudinal emittances.

Figure 19 and 20 are from an Elegant simulation of the remainder of the NLCTA beamline, starting at the exit of the first 0.9 m x-band accelerator section, proceeding through the chicane, modified matching section, six 1.8 meter long x-band structures, the NLCTA spectrometer magnet, and ending at the wire scanner downstream of the spectrometer. No hardware reconfiguration is required to obtain the cases shown. The NLCTA chicane has been appreciably retuned to reduce emittance growth in the dispersive plane. The relatively large momentum spread ($\delta p/p_o \sim 10^{-3}$) combines with the strong quadrupole gradients and large horizontal beta functions to generate strong second order aberrations that badly degrade the horizontal emittance. This has been partially addressed here by tuning for moderate beta functions and low

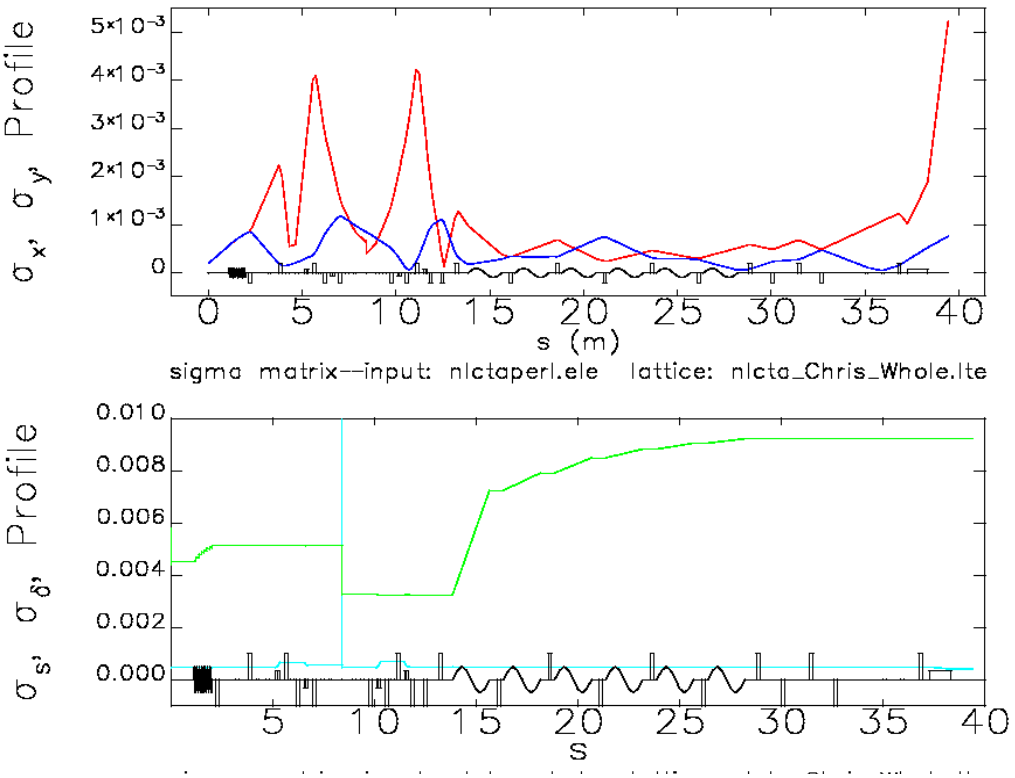

FIGURE 19. Elegant simulation of 1 nC beam transport through the NLCTA, beginning from the exit of the first accelerator section, and proceeding to wire scanner WIRE2270 after the NLCTA spectrometer. Top: horizontal (red) and vertical (blue) envelopes, bottom: energy spread (green) and bunch length (blue).

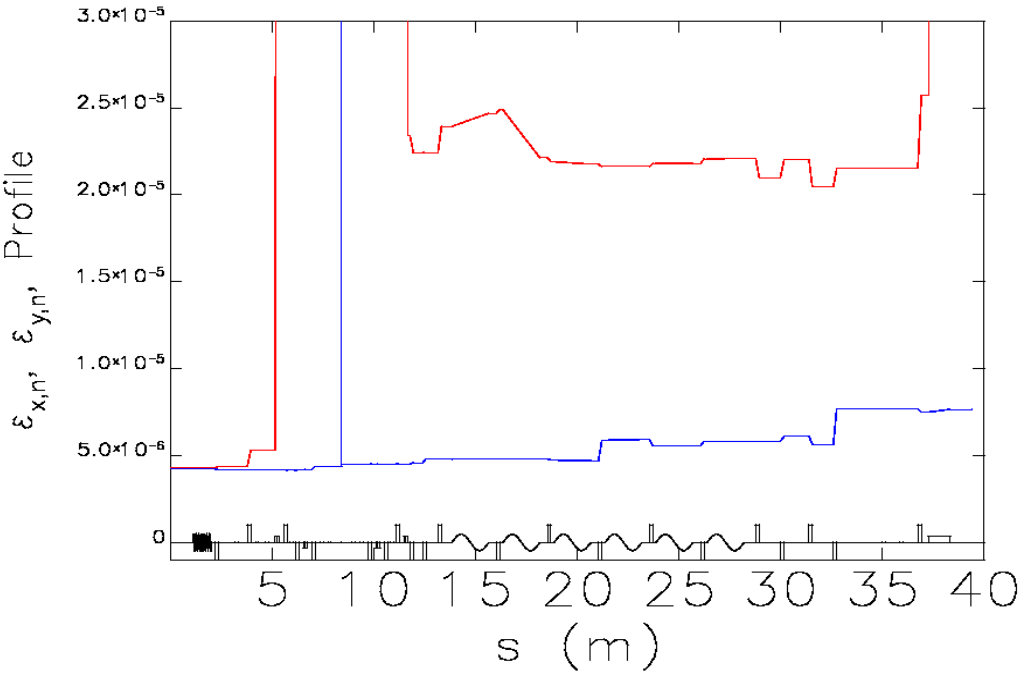

FIGURE 20. Elegant simulation of normalized emittances of 1 nC bunch transported through NLCTA. Strong chromatic aberrations in the chicane degrade the horizontal emittance by a factor of 5.

quadrupole gradients, at the expense of making the chicane temporally dispersive again, R_{56}=-4.9 cm. As is visible in Figure 18 below, there is no penalty in the bunch peak current, provided the upstream accelerators are phased to yield a correlationless longitudinal distribution.

Simulations show that 60 MeV, 1 nC bunches with 4x4 π mm-mr emittances may be produced from the injector with a 300 keV RMS energy spread and 1.4 ps RMS bunch length, corresponding to a peak current of 285 Amps. Upon transport through the chicane, a beam of 850 pC, $\delta p/p_o$=0.003, σ_t=1.4 ps (241 Amps), 23 x 5 π mm-mr beam is produced and can be transported through the subsequent x-band accelerators without loss.

Future Potential

In the development of the experiment other possible ways to proceed will become evident and we will pursue them. Two that are under consideration are the continued development of high damage threshold materials and the use of shorter laser pulses.

Materials with improved laser damage threshold performance will permit higher fluences and higher acceleration gradients. We will continue to work with industry to uncover higher damage threshold materials and test them, and will explore the use of different substrates (silicon in particular), as the surface quality is known to influence the quality of the overlying dielectric coating.

There is also the readily explored possibility of using shorter laser pulses, as discussed in the appendix to the E163 proposal, to capitalize on the independence of the damage threshold fluence on pulse length for pulse lengths below 1 psec. The shorter pulse will allow greater acceleration gradients, but over a smaller portion of the electron bunch, resulting in a larger "spectator" population. This would produce a small population of electrons whose energy spread far exceeds the natural energy spread of the incoming bunch, producing a signature that is unique, provided that the relatively smaller population of accelerated electrons can be successfully discerned from the spectators.

Conclusions

The experiments proposed in E163 place requirements on the stability and quality of the electron source that are similar in many respects to those of a linear collider, as with the requirements for reasonable transverse emittances and freedom from excessive jitter and drift. The unusual requirements derive from the small extent of the longitudinal phase space admitted by the laser accelerator. A reduction in bunch charge and the use of a high quality rf gun permit bunches with RMS energy spreads and bunch lengths already almost suitable for the experiment at 30 keV and 130 μm RMS, respectively. Modest energy collimation is enough to provide the final required improvement in beam quality, and serves to "veto" pulses that would otherwise have sizable variation in energy spread (hence mimic the experimental signature) because these pulses also tend to have quite different centroid energies. Additionally, electron/laser timing variation caused by time-of-flight differences of differing energy electron bunches will similarly be reduced by collimation.

It is clear that the main penalty of collimation is the introduction of severe charge jitter, which does not mimic the experimental signature, but which does lower the data acquisition rate. We have shown that by measuring the charge of the collimated bunches we can veto off-energy off-time pulses with good discrimination, permitting cleaner experimental data sets to be acquired, albeit at reduced data rate. Nor does the reduction in charge of the good pulses pose a problem as these pulses have significantly more charge than the bunches we routinely diagnose and perform high resolution spectrometry on at HEPL.

Reducing the phase jitter and amplitude jitter of the rf sources will clearly improve the data rate, and there is potentially room for improvement. Pulse-to-pulse modulator voltage stability of $\delta V/V$=0.001 has been

measured[7], which translates to a voltage stability in the accelerator structures of 0.00125, and a phase stability of 2^{o} RMS (0.50 ps) at x-band, factors of 8 and 2, respectively, below the values used in calculations here.

Vacuum laser acceleration has the potential for extraordinary gradients using technologies being aggressively developed by industry. E163 proposes proof-of-principle tests that are the first steps to realize this potential. The demands of the E163 experimental program are consistent with the state-of-the-art performance of electron sources, and are achievable. We have shown a route by which the NLCTA may be upgraded to meet these demands while maintaining sufficient flexibility to accommodate future NLC experiments. Indeed, the experimental facility that will be constructed for E163 will be broadly useful for other advanced accelerator R&D experiments requiring well-diagnosed high quality electron and laser beams.

References

[1] W. Graves, "Sub-picosecond measurements of photoinjector electron beam properties", talk presented at the LCLS TAC meeting, December, 2001.
[2] C. Adolphsen, Transport input file dated May 12, 1995.
[3] NLC ZDR, SLAC-474, May, 1996.
[4] R. Gluckstern, *Phys. Rev. D*, **39**, p. 2780, (1989).
[5] P. Sprangle, E. Esarey, J. Krall, A. Ting, *Opt. Comm.* **124**, p.69-73, (1996).
[6] J. Rosenzweig, E. Colby, "Charge and Wavelength Scaling of RF Photoinjectors: a Design Tool", in Proc. IEEE Part. Accel. Conf., Dallas, TX, p.957ff (1995).
[7] A. Vlieks, private communication.